

# How Succolarity could be used as another fractal measure in image analysis

R.H.C. de Melo · A. Conci

© Springer Science+Business Media, LLC 2011

**Abstract** Three aspects of texture are distinguished by fractal geometry: Fractal Dimension (FD), Lacunarity and Succolarity. Although, FD has been well studied and Lacunarity has been more and more used, Succolarity, until now, has not been considered. This work presents a method to compute Succolarity. The proposed approach, for this computation, is based on the evaluation of a proposed equation that employ the FD Box Counting idea adapted to the concept of Succolarity. Simple examples, on 2D and 3D images, are considered to easily explain, step by step, how to compute the Succolarity. To illustrate this approach examples are shown, they range from satellite to ultrasound images. The proposed form of Succolarity evaluation is a unique feature usable whether it is relevant differentiate images with some directional or flow information associated with it. Therefore it could be used as a new feature in pattern recognition processes for the identification of natural textures. Furthermore, it works very well when is relevant differentiate images with some characteristics (e.g. directional information) that can not be discriminate by FD or Lacunarity.

**Keywords** Succolarity · Fractal measure · Percolation · Binary analysis · 3D analysis

---

R.H.C. de Melo  
ADDLabs, UFF—Federal Fluminense University, Av. Gal. Milton  
Tavares de Souza, s/n°, Niterói, 24020-240, Rio de Janeiro, Brazil  
e-mail: [rhc\\_melo@gmail.com](mailto:rhc_melo@gmail.com)

A. Conci (✉)  
Computer Institute (IC), UFF—Federal Fluminense University,  
R Passo da Pátria 156, Bloco D/452 Niteroi, 24210-240,  
Rio de Janeiro, Brazil  
e-mail: [aconci@ic.uff.br](mailto:aconci@ic.uff.br)

## 1 Introduction

The here proposed approach to calculate Succolarity is a natural evolution of the others well known fractal measures evaluators: FD and Lacunarity. These two measures already have good and effective computation methods. Our goal is propose a simple method that attend to the notions of Succolarity [1] and preserve similar characteristics of the already known measures.

These three FD measures are complementary: That is, two sets could have the same FD and be distinguished by Lacunarity [2]. On the same way, the idea of Succolarity makes possible distinguish different sets or textures that have the same FD and Lacunarity [3] or vice-versa. The Fractal Dimension indicates how much an object occupies its underlying metric space. An intuitive definition of Lacunarity is that it measure the gap (or lacuna from Latin) distribution [4]. A fractal is more lacunar if its gaps tend to be large, in the sense that they include large intervals (discs, or balls). The Succolarity [1] indicates the capacity of a flow to cross the set. A Succolarity on fractal sets is defined as evaluation of the degree of filaments that allow percolation or to flow through. Methods to calculate FD were implemented in a great number of applications [5–10]. There are also a number of works on Lacunarity computation [3, 4, 11, 12]. The algorithm here proposed was based on the box counting method [6] adapted to the notions of Succolarity [13]. Pressure of a virtual fluid was considered to evaluate the relation among direction and percolation, on the result. The input of the approach, here explained, must be binary images.

A completely novel expression to compute Succolarity is presented here, as well as a totally new computation approach. The only definition for this measure that we use is a descriptive one presented by Mandelbrot. Therefore, a formal definition and an original approach are both proposed.

$$\text{FD} \left( \begin{array}{c} \text{243x243} \\ \text{Sierpinski's carpet} \end{array} \right) = \text{FD} \left( \begin{array}{c} \text{81x81} \\ \text{Sierpinski's carpet} \end{array} \right) = \text{FD} \left( \begin{array}{c} \text{27x27} \\ \text{Sierpinski's carpet} \end{array} \right) \approx 1.89$$

**Fig. 1** Comparison of Fractal Dimension of Sierpinski's carpet with different resolutions:  $243 \times 243$ ,  $81 \times 81$  and  $27 \times 27$  pixels.  $\text{FD} = \log(8)/\log(3) \approx 1.89$ . Fractal Dimension does not change with scale

The method is based on the box counting approach [5] but with adaptations to attend the notions of Succolarity [13]. This text could then be a basic tutorial for people who would like to use this. Simple examples are used to explain, by stages, how to compute the Succolarity for binary images and for 3D objects.

To illustrate, the approach is used to characterize satellite images of cities through its social aspects [11, 12, 19], and to evaluate blood circulation in biomedical images [2]. Another type of application that demonstrate to be interesting to future investigations is the analysis of the texture appearance of pre-sliced pork ham images to characterize its qualities [20].

## 2 Why another fractal measure, like Succolarity could be useful?

The main idea of this section, is to explain, through examples, the necessity of using, not just one, but a combination of fractal measures, to help the identification of texture patterns on images. The three fractal characteristics (fractal dimension, Lacunarity and Succolarity) explore different aspects of the images in a complementary way. Two images could present the same Fractal Dimension but different Lacunarity; or the same Lacunarity but different Succolarity; and any other combination of results.

The Fractal Dimension (FD) is a measure that characterizes how much an object occupies the space that contains it. FD is a measure that does not change with scale neither with translation nor rotation. Through examples in Figs. 1 and 2 some of these aspects can be observed. Lacunarity measures the size and frequency of gaps on the image. Succolarity measures how much a given fluid can flow through an image, considering as obstacles the set of pixels with a defined color (e.g. white) on 2D images analysis.

### 2.1 Fractals with the same Fractal Dimension and Lacunarity but different Succolarity

The Fractal Dimension, in some cases, is not enough to differentiate texture of images. The Fractal Dimensions of the two fractals in Fig. 3 are equal. Nevertheless, it is easily shown by its definitions, that the Succolarity of those images are different. This is shown in Figs. 4 through 7.

$$\text{FD} \left( \begin{array}{c} \text{image} \\ \text{Sierpinski's carpet} \end{array} \right) = \text{FD} \left( \begin{array}{c} \text{image rotated 90° CW} \\ \text{Sierpinski's carpet} \end{array} \right) \approx 1.89$$

**Fig. 2** Comparison of FD of a fractal with the same Fractal Dimension of Sierpinski's carpet rotated ninety degrees clockwise. Fractal Dimension does not change with rotation

$$\text{FD} \left( \begin{array}{c} \text{Sierpinski carpet} \end{array} \right) = \text{FD} \left( \begin{array}{c} \text{8 parts fractal} \end{array} \right) = \frac{\log(8)}{\log(3)} \approx 1.89$$

**Fig. 3** Two different fractals with the same FD. Sierpinski carpet and another fractal with the same rule of construction: 8 parts with a scale factor of  $1/3$

**Table 1** Numerical results of the  $\ln \times \ln$  Succolarity plot for Fig. 7

$\ln(d)$	$\ln(100 \times \sigma)$			
	b2t	t2b	l2r	r2l
4.9053	4.1236	4.1236	4.3655	4.3655
3.8067	4.1241	4.1241	4.3651	4.3651
3.2958	4.1236	4.1236	4.3655	4.3655
2.7081	4.1249	4.1249	4.3644	4.3644
2.1972	4.1340	4.1340	4.3572	4.3572
1.6094	4.1270	4.1270	4.3627	4.3627
1.0986	4.1648	4.1648	4.3319	4.3319

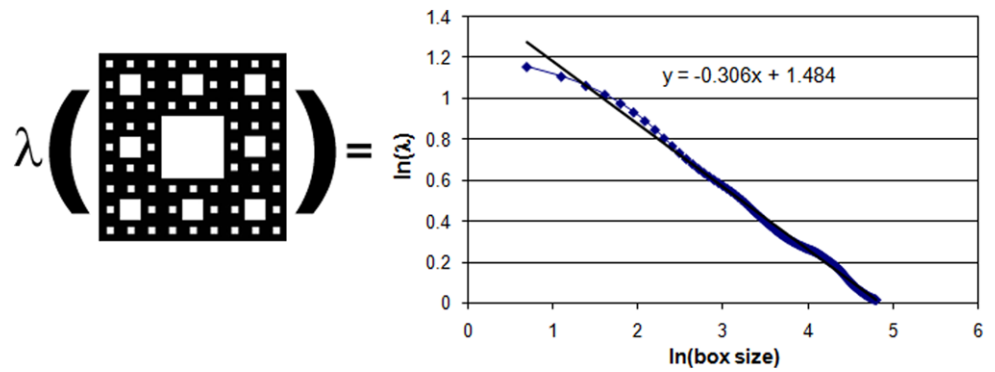
Figures 4 and 5 illustrate that the fractals in Fig. 3 have almost the same values of Lacunarity.

The small differences can be better seen when analyzing the slope of the line that has the best curve fit to the points of bi logarithm plot of Lacunarity over the box sizes, while in Fig. 4, this value is approximately  $-0.31$ , in Fig. 5, this value is approximately  $-0.29$  as the equations of the lines shown.

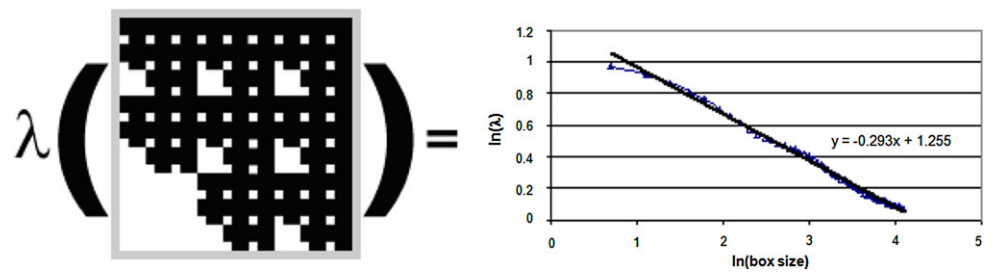
In Figs. 6 and 7, the difference on the results of Succolarity is easily shown by the  $\ln \times \ln$  plots, since the Sierpinski carpet (in Fig. 6) is a totally symmetric fractal, producing equal results in the four directions of analysis of the Succolarity. The fractal in Fig. 7 is only half symmetric, as it can be seen in the bi logarithm plot in this figure and by the results in Table 1.

Table 1 shows in the first column the logarithm of the dividing factor of the boxes and on the second column the logarithm of the Succolarity times 100. The sub-columns illustrate respectively the results for the directions: bottom to top (b2t); top to bottom (t2b); left to right (l2r) and right to left (r2l). The results in this table made clear that the Succolarity for this image does not change by reversing the direction through the same axis.

**Fig. 4**  $\ln \times \ln$  plot result of Lacunarity of Sierpinski carpet



**Fig. 5**  $\ln \times \ln$  plot result of Lacunarity of a fractal with the same FD of the Sierpinski carpet



**Fig. 6** Succolarity of Sierpinski carpet

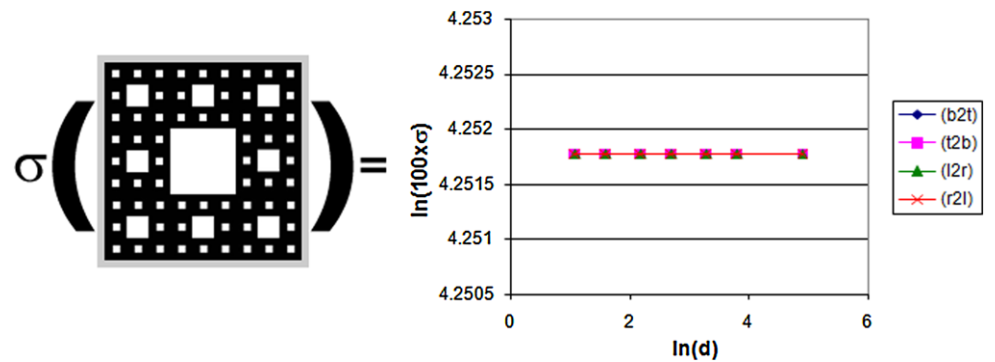
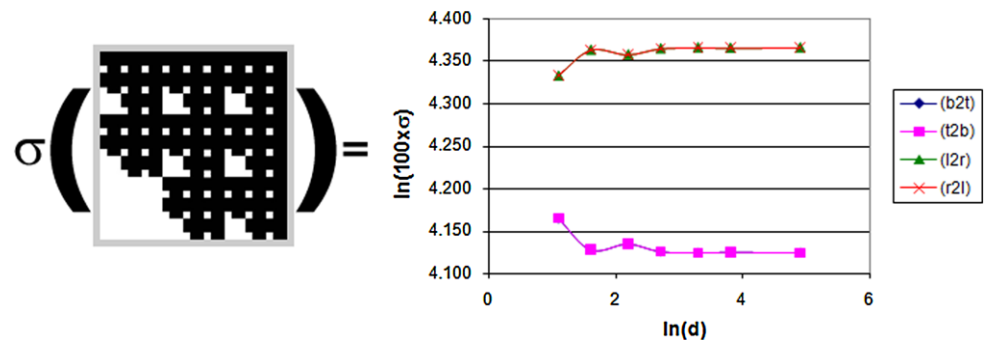


**Fig. 7** Succolarity of a fractal with the same FD of the Sierpinski carpet



### 3 An approach to measure Succolarity

Succolarity measures the percolation degree of an image (how much a given fluid can flow through this image). To evaluate this, consider the image in Fig. 8(a). Suppose that each pixel position can be considered as empty (black pixels) or with impenetrable mass (white pixels). Let us simulate the draining or percolation capacity of a fluid through

the image. From the image to be analyzed, Fig. 8(a), we obtain, depending on the directions to be considered, Fig. 8(b), two or more images (Fig. 9). On the example in Fig. 8 four images (Fig. 9) were obtained, the original image was analyzed flooded vertically (top to bottom and bottom to top) and horizontally (left to right and right to left). Other directions can be applied to generate different overflowing images, if representative, as well.

Additionally to the fluid direction a pressure field is supposed. The idea of pressure applied to a box is demonstrated in Fig. 10. The pressure field grows from top to bottom on the vertical case (directions: Top to bottom (t2b); and bottom to top (b2t)) and from left to right on the horizontal case (directions: Left to right (l2r) and right to left (r2l)). The arrows in Fig. 10 represent these. Also, as the previous fractal measures it presents scaling property. One can estimate the Succolarity of the set by covering it with boxes of various sizes.

There are two ways to divide the image of Fig. 8(a) in equal sized boxes. With a dividing factor,  $d$ , of 3 obtaining boxes of  $3 \times 3$  pixels and by  $d = 9$  obtaining boxes of  $1 \times 1$  pixels (only considering integer divisions and without considering the dividing factor of 1 of course). These two examples are in Fig. 11.

### 3.1 Describing the method through a top to bottom analysis of an image

The approach to calculate Succolarity can be explained by the four next steps:

*Step 1)* Coming from the top of the original binary image, all the black pixels are considered empty on the image (in our case we consider black as the absence of elements in the pixel position), it means that a fluid can pass and flood this area. The existing material (white pixels on the example) are considered as obstacles to the fluid. All the flood areas

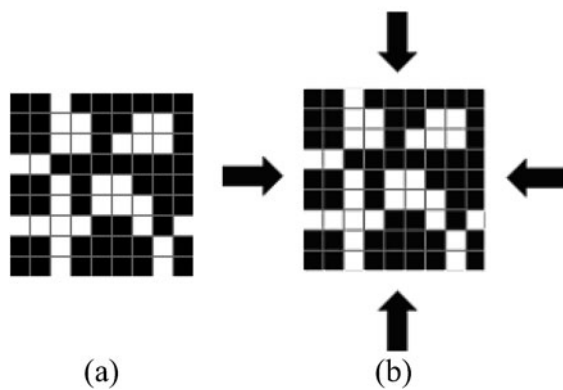
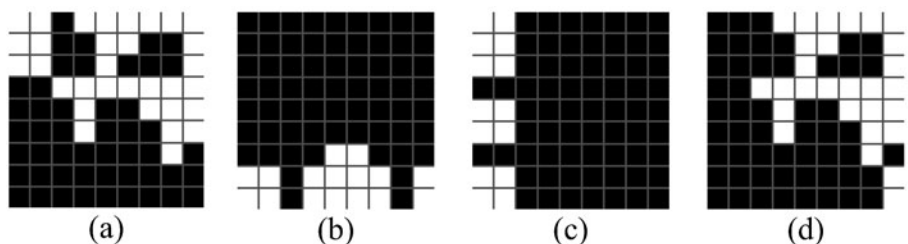


**Fig. 8** (a) Original image (9 × 9): black pixels represent empty position or gaps; (b) Example of four considered directions that a fluid can try to flood the image

**Fig. 9** Images obtained after the first step of the Succolarity. In white the flood from: (a) Top to bottom (t2b); (b) Bottom to top (b2t); (c) Left to right (l2r); (d) Right to left (r2l)



from a boundary have their neighbors (4 neighbors for each pixels: Top; Bottom; Left and Right) considered on the next step and this process is recursively executed.

*Step 2)* The next step is then to divide these flood area of each image (Fig. 11) in equal box sizes ( $BS(k)$ , where  $k$  is the number of possible divisions of an image in boxes) like the box counting method. After that the occupation percentage ( $OP$ ) is measured in each box size of each image, this is denoted  $OP(BS(k))$ . The evaluation of the occupation percentage is demonstrated in the examples sketches in Fig. 12.

*Step 3)* For each box size,  $k$ , the expression in (1) is evaluated:

$$\sum_{k=1}^n OP(BS(k)) \times PR(BS(k), pc) \tag{1}$$

Where  $OP(BS(k))$  is obtained from step 2,  $n$  is the number of possible divisions and  $PR(BS(k), pc)$  represent the pres-

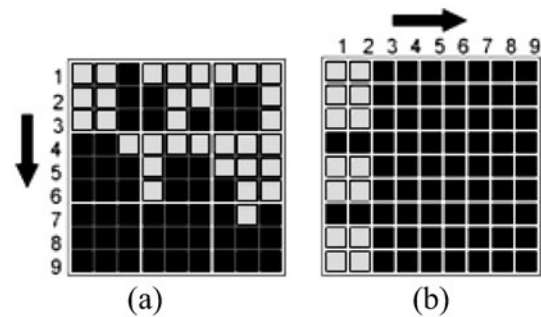


**Fig. 10** Indication of the increasing pressure over the boxes: (a) Example of pressure over  $3 \times 3$  boxes for Fig. 9(a); (b) Example of pressure over  $1 \times 1$  boxes for Fig. 9(c)

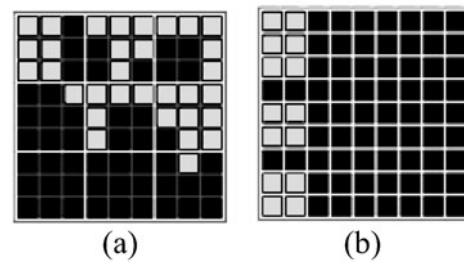


**Fig. 11** Dividing the intermediate images of Fig. 9 in boxes of two different sizes: (a) Fig. 9(a) with  $d = 3$ , producing boxes of size  $3 \times 3$  pixels; (b) Fig. 9(c) with  $d = 9$ , producing boxes of  $1 \times 1$  pixels

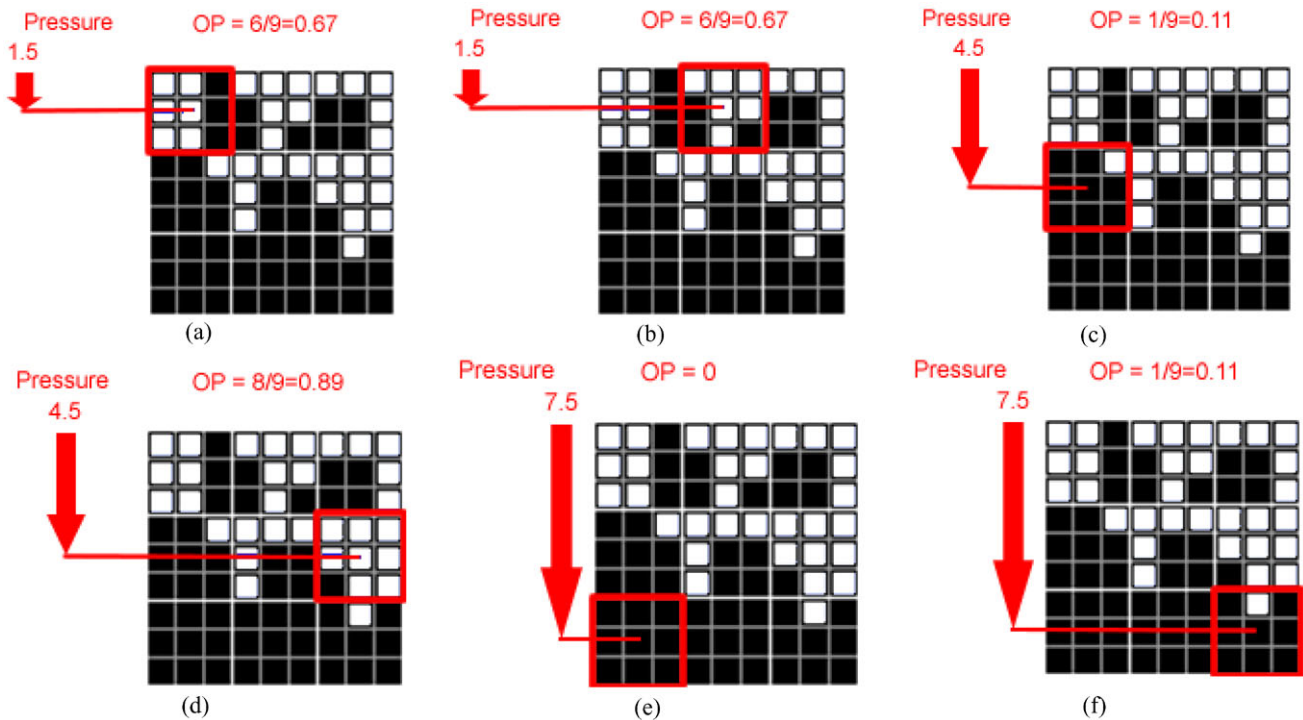


**Fig. 12** Evaluation of the occupation percentage,  $OP(BS(k))$ , of some boxes when the Succolarity have as input the image in Fig. 10(a). The pressures over the boxes are also shown

sure over the centroid of the box  $k$  on the scale on consideration. This could be obtained by the  $x$  (in the horizontal case) or  $y$  (vertical case) coordinates of the centroid. The pressure varies with the box size because it is applied on the centroid of the box. It also depends on the position of the box to correctly indicate the amount of pressure over it, as indicated in Fig. 12.

The pressure (Figs. 10 and 12) is over the centroid of the box. Then there is horizontal field of pressure, the  $x$  position of the centroid is used while on the vertical case the  $y$  position is considered.

*Step 4)* To make the Succolarity value dimensionless like FD and Lacunarity we divide the value, obtained in (1), by its larger possible value, that is now considering that the image was totally flooded by the fluid (as if the input image were totally black). The calculation is indicated in (2).

$$\sigma(BS(k), dir) = \frac{\sum_{k=1}^n OP(BS(k)) \times PR(BS(k), pc)}{\sum_{k=1}^n OP(BS(k)) \times \max PR(BS(k), pc)} \quad (2)$$

where  $dir$  represent the direction, for instance, left to right.

### 3.2 How to calculate the percentage of occupation as well as the pressures over it

The image of Fig. 11(a) was used here, as input, to illustrate the evaluation of the percentage of occupation,  $OP(BS(k))$ , of some boxes and the pressure over them,  $PR(BS(k), pc)$ .

In image of Fig. 12(a), six pixels are occupied over a total of nine pixels to the hole box, then the occupation percentage,  $OP(BS(1))$ , considering this, the first box evaluated is  $6/9 = 0.67$ . The pressures over the centroid of the boxes are also shown on all the images, in this first image, the pressure is of 1.5. The result of the image in Fig. 12(e) is  $OP(BS(7)) = 0$ , because there are not pixels occupied, the pressure over the box is 7.5 as could be seen on the image.

### 3.3 Example of the calculus of Succolarity

This section computes, using the steps of last section, Succolarity for Fig. 11.

#### 3.3.1 Box size equal to 1 pixel—direction left to right

In Fig. 11(b), each box corresponds to a pixel, the occupation percentage then could be only 0 (pixel without fluid) or 100% (pixel with fluid). On this figure we can easily note that 14 boxes have 100% of occupation and the others 67 boxes have 0%. The  $x$  positions of the centroid are the same for all of the boxes on the same column in the case of the horizontal percolation (the same occurs with the lines on the vertical percolation). The  $x$  value of the centroid is then 0.5 for the boxes on the first column and 1.5 for the second (considering the pressure distribution like

**Table 2** Results of the Succolarity of Fig. 8(a)

$d$	$BS$	Succolarity ( $\sigma$ )			
		b2t	t2b	l2r	r2l
9	(1 × 1)	0.3429	0.2387	0.0384	0.4829
3	(3 × 3)	0.3292	0.2634	0.0576	0.4691

Fig. 10(b)). Figure 11(b) presents 7 boxes on the first column and 7 more on the second. We have then using the numerator of (1) obtained the results  $7 \times 0.5 + 7 \times 1.5 = 14$ . To compute the Succolarity we then divide this value by the denominator of (2). This calculus results in  $364.5 (= 9 \times (0.5 + 1.5 + 2.5 + 3.5 + 4.5 + 5.5 + 6.5 + 7.5 + 8.5))$ , as the 9 columns suffer pressures between 0.5 to 8.5 and there are 9 boxes on each column. The Succolarity value for the box size  $1 \times 1$  is then  $\sigma(1 \times 1; l2r) = 14/364.5 \approx 0.0384$ .

### 3.3.2 Box size equal to 9 pixels (3 × 3)—direction top to bottom

In Fig. 11(a) each box correspond to  $3 \times 3$  pixels; to calculate the percentage of presence of each box is necessary to divide the number of filled pixels on the box by the area of that box (9 in this case). Figure 11(a) shows 7 boxes with some percentage of occupation and 2 with 0%. The upper left box has 6 pixels, the percentage of that boxes is then  $6/9 \approx 0.67$ . The percentages of occupied boxes of the top of the image respectively from left to right are 0.67, 0.67 and 0.56 ( $\approx 5/9$ ), that is, a total of 1.90; on the middle boxes this percentages are 0.11 ( $\approx 1/9$ ), 0.56 and 0.89 ( $\approx 8/9$ ), a total of 1.56; and on the bottom boxes there are 0, 0 and 0.11. Considering the pressure like in Fig. 10(a), the  $y$  position of the centroid is 1.5 on the three boxes of the top, 4.5 on the three middle boxes and 7.5 on the 3 boxes on bottom of the image. The maximum value possible by a  $9 \times 9$  image with  $3 \times 3$  boxes completely flooded is  $(1.5 + 1.5 + 1.5 + 4.5 + 4.5 + 4.5 + 7.5 + 7.5 + 7.5) = 40.5$ . This value can be seen as the sum of the maximum “pressure” applied to each box. The Succolarity value is then easily determined by the simple application of (1).  $\sigma(3 \times 3, t2b) \approx (1.5 \times 1.90) + (4.5 \times 1.56) + (7.5 \times 0.11)/40.5 \approx 0.2634$ .

All the results of the Succolarity of Fig. 8(a) are shown in Table 2.

### 3.4 Example of the 3D approach

Figure 13 shows the 3D synthetic image used to illustrate the approach of measuring the Succolarity of 3D images or objects. In this image, the voxels are represented as cubes: yellow cubes (including the transparent ones) represent the obstacles to the fluid while the blue cubes already represent the areas where the fluid percolates the image. Figure 14

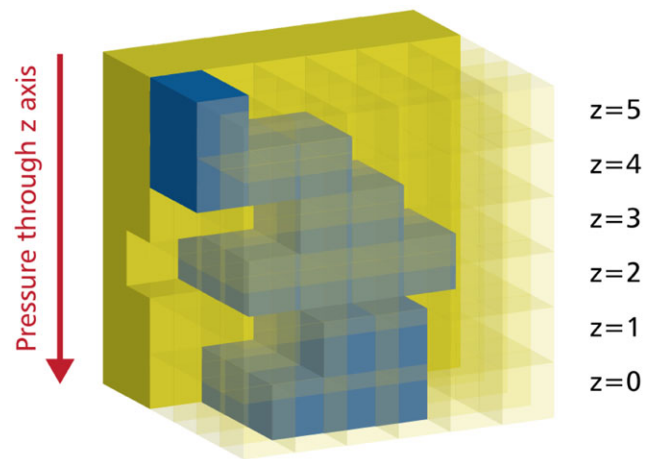


**Fig. 13** 3D Synthetic image used already with the representation of the percolation of fluid (in blue)

shows the 2D slices that forms the 3D synthetic image in Fig. 13. In these images (Fig. 14), the black squares represent the empty voxels corresponding to the paths that the fluid can flow from the top to the bottom slice of the image. The white squares represent the voxels in the image that corresponds to the obstacles to the fluid flow through the image.

The pressure field through the new axis ( $z$ ) grows from top to bottom, as represented in Fig. 13, then the pressure over the first slice (Fig. 14(a),  $z = 5$ ) is smaller than the pressure on the second slice (Fig. 14(b),  $z = 4$ ) and so on to the greater pressure that is applied on the last slice (Fig. 14(f),  $z = 0$ ).

The dimension of the image represented by the slices in Fig. 13 is  $6 \times 6 \times 6$ : 6 pixels wide; 6 pixels high and 6 pixels depth. This image has then three possibilities of division: factor of division 2, 3 or 6, having respectively boxes sizes of:  $3 \times 3 \times 3$ ;  $2 \times 2 \times 2$  and  $1 \times 1 \times 1$  pixels.

For the box of size  $1 \times 1 \times 1$  we have pressure values through the slices from 0.5 to 5.5. Considering “slice  $n$ ” as the slice where the value of  $z = n$ ; the pressure is 5.5 on slice 0. Then we have 2 boxes with pressure 0.5 (slice 5); 6 boxes with pressure 1.5 (slice 4); 4 boxes with pressure 2.5 (slice 3); 10 slices with pressure 3.5 (slice 2); 6 boxes with pressure 4.5 (slice 1); and 9 boxes with pressure 5.5 (slice 0). Considering (1) and that with boxes of  $1 \times 1 \times 1$  the boxes are 0 or 100% occupied, the result of Succolarity for box size  $1 \times 1 \times 1$  is  $\sigma(1 \times 1 \times 1, t2b) \approx 131.5/648 \approx 0.2029$ .

For the box size  $2 \times 2 \times 2$  we have pressure through slices from 1 (slice 4 and 5) to 5 (slice 0 and 1). On slices 4 and 5 we have 2 boxes partially occupied: one with occupation of 75% and the other with 25%. Slices 2 and 3 (with pressure 3 over them) have 5 boxes with some occupation: 2 with 12.5%; 2 with 25% and 1 with 100% of occupation. Slices 0 and 1 have 4 boxes partially occupied: 1 with 12.5%; 1 with 25%; 1 with 50% and 1 with 100% of occupation. Considering (1) and the pressure and occupations

**Fig. 14** Representation through slices of the 3D synthetic image used as input for the 3D approach of the Succolarity: from the upper slice on (a)  $z = 5$  to the bottom slice on (f)  $z = 0$

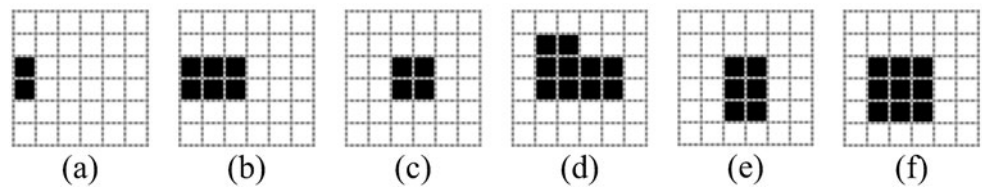


**Table 3** Numerical results of the Succolarity for the 3D synthetic image represented by in Fig. 13

$d$	$BS$	Succolarity ( $\sigma$ ) $t2b$
6	$(1 \times 1 \times 1)$	0.2029
3	$(2 \times 2 \times 2)$	0.1929
2	$(3 \times 3 \times 3)$	0.2012

measured we have the result of Succolarity for this box size of  $\sigma(2 \times 2 \times 2, t2b) \approx 15.625/81 \approx 0.1929$ .

With the box size  $3 \times 3 \times 3$  we have pressure through slices from 1.5 (slices 3, 4 and 5) and 4.5 (slice 0, 1 and 2). On slices 3, 4 and 5 we have 4 boxes partially occupied: 2 with occupation of 3.7% and the two other with 18.5%. Slices 0, 1 and 2 have also 4 boxes with some occupation: 1 with 14.8%; 1 with 22.2%; 1 with 25.9% and 1 with 29.6% occupation. Considering (1) and the pressure and occupations measured, we have the Succolarity for this box size as  $\sigma(3 \times 3 \times 3, t2b) \approx 4.8285/24 \approx 0.2012$ .

The numerical results of Succolarity are shown in Table 3.

### 4 Experiments on real images

To display that the Succolarity is, like the other fractal measures, a powerful method to characterize real images, we apply, in this section, the Succolarity method on satellite images of cities and on medical images too.

#### 4.1 Application of Succolarity in the characterization of social aspects of cities

Considering that cities are systems with fractal features because they are the result of a dynamic system with complex logic, whose patterns cannot be measured by usual concepts and tools from classical geometry [15–17, 21, 22]. We use here these types of images as input to Succolarity evaluation. The idea is to demonstrate the results of Succolarity as a complementary measure to Lacunarity, as well as Lacunarity was demonstrated to be complementary to Fractal Dimension measures in lots of cases [11, 12].

The particular problem of characterizing social aspects of cities and differentiate informal and formal areas fit very

well to the concepts of Succolarity. Normally a great difference between formal and informal areas lies on the width of the streets, bigger on the formal area. Also, quite often the alleys that exist on informal areas do not communicate with neighboring streets. This could be better explained if one could imagine that is not as easy for a car to drive through all the parts of an informal area like it is in a formal area.

To better illustrate the results, the images used here were images already used and discussed on previous works [11, 12]. These papers use Lacunarity to distinguish the spatial configuration of slums from formal areas as well as from other regions to contribute for the development of alternative and complementary classifications of settlements. The goal is to generate complementary mapping and classifications for city planning through satellite images.

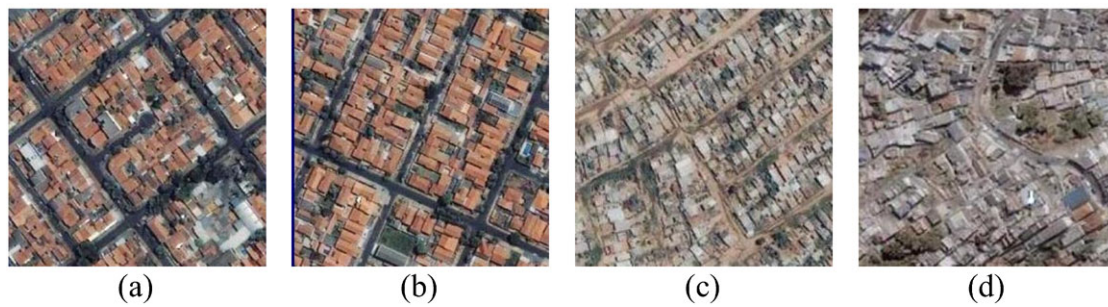
The images used here (including the binary version of each image) were gently sent by the authors of the paper [11] (Figs. 15 and 16). The image in Fig. 16(c) is the inverted version of the image sent by them to ensure that the results present proper behavior. These satellite images were originally captured by the IKONOS [18] and its images could be freely downloaded through the internet for non-profit research and evaluation purposes.

Four images were used for this analysis (Fig. 15), three from the city of Campinas, SP, Brazil: two regular (orthogonal geometry) samples and on irregular (slum) sample, and one image, with an irregular sample, from the city of Rio de Janeiro, Brazil. All images here have  $270 \times 270$  pixels.

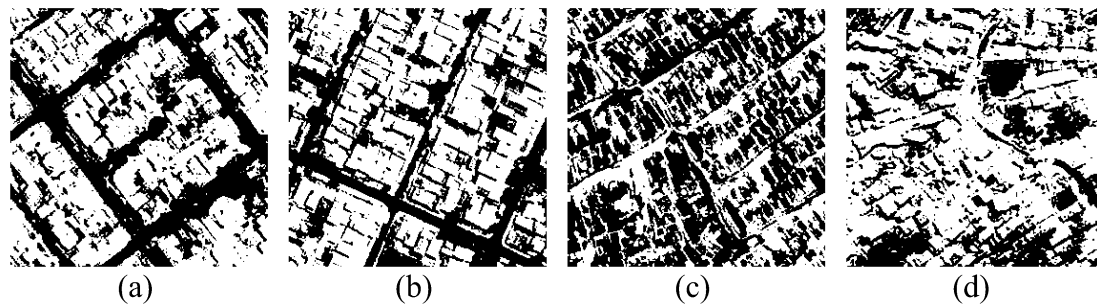
The images in Fig. 16 were thresholded in such a way that the constructions (obstacles that do not permit percolation) in Fig. 15 are mainly represented in white while the streets (areas that permits percolation) are mainly represented in black. For that, we inverted (each pixel black became white and vice-versa) one of the images (correspondent to the binary image of Fig. 15(c)) reaching in Fig. 16(c), because in all other images the black pixels represent the streets and the white ones represent the constructions, like we expect.

Figure 17 shows a plot with the mean result of the Succolarity (this is a simple average of the four directions of Succolarity analysis: left to right, right to left, top to bottom and bottom to top) for the three images from Campinas.

Figure 18 illustrates the gain of using the Succolarity over the Lacunarity for this example. The informal areas, as can be seen through the results, produce well separated graphs, demonstrating that Succolarity is a good measure to characterize this kind of pattern.



**Fig. 15** Satellite images from IKONOS: (a) and (b) two regular samples of occupation from Campinas: (a) formal 1 and (b) formal 2; (c) informal 1: slum of Campinas; (d) informal 2: slum from Rio de Janeiro



**Fig. 16** Binary version of images in Fig. 15

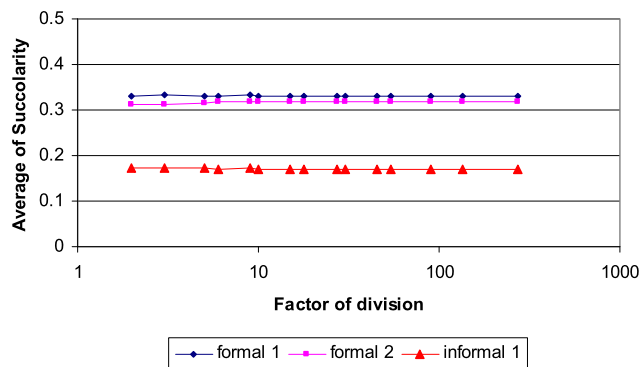


**Fig. 17** Results of Succolarity medium obtained from the proposed method using as input the images of Campinas in Fig. 16(a) formal 1, (b) formal 2 and (c) informal 1

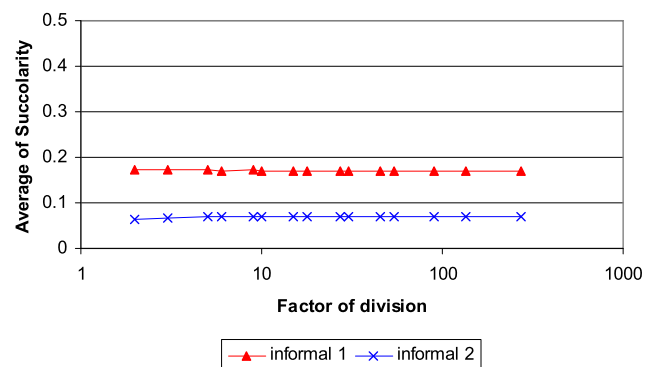


**Fig. 18** Results of Succolarity medium obtained from the proposed method using as input the images of Campinas in Fig. 16(c) informal 1 and 16 (d) informal 2

Another important point here, is that, this results are the arithmetic mean results of Succolarity in a way that, for specific application, as we will see on the next section, only one or a particular number of directions could be measured, as it are considered interesting for the problem to be solved.

On plots of Figs. 19 to 22 one could see that, through other type of analysis, the results of Succolarity could be used to distinguish formal areas through informal ones. These results consider four directions that a fluid can flood the original images: bottom to top (b2t); top to bottom (t2b); left to right (l2r); right to left (r2l). Figures 19 and 20 demon-

strate that, on formal areas, the results do not vary considerably with the direction. This is easily explained when we think that formal areas usually have a great number of large streets that go from lots of points to others including points where some streets cross others.

Figures 21 and 22, which are results of Succolarity of informal areas, demonstrate that, in this kind of occupation, the direction used on the evaluation makes great impact on the results. While, for the analyzed formal areas, the minimum values of Succolarity evaluated are on decimals for the informal areas, the minimum values are in hundredths, which is better seen next; in Tables 4, 5, 6 and 7 (the val-

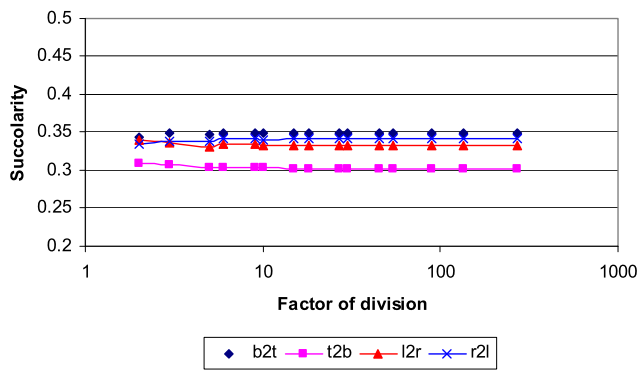


Fig. 19 Results of Succolarity of the image in Fig. 16(a)—formal 1

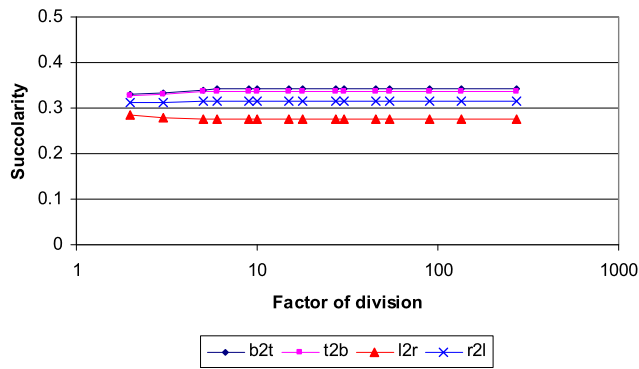


Fig. 20 Results of Succolarity of the image in Fig. 16(b)—formal 2

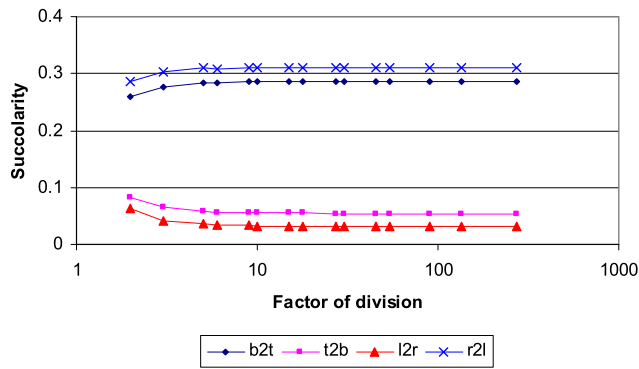


Fig. 21 Results of Succolarity of the image in Fig. 16(c)—informal 1

ues on tables were multiplied by ten to make the values more readable). Another consideration is that the maximum difference between the measures that on formal areas are around hundredths, in informal areas this difference grows considerably to decimals.

#### 4.2 Application of Succolarity to medical images

An application of the Succolarity to vascular diagnosis is shown in this section. The two examples of images [14] demonstrate a carotid with and without occlusion. On first

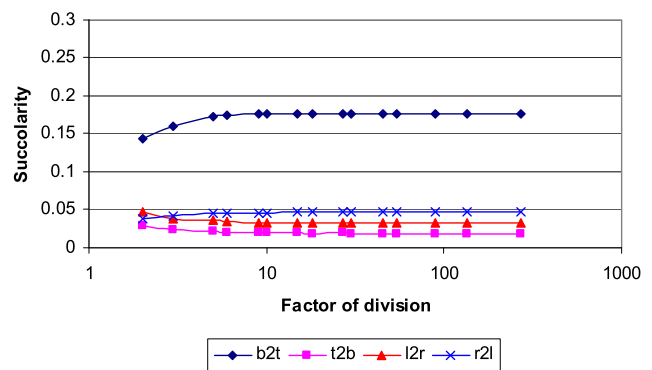


Fig. 22 Results of Succolarity of the image in Fig. 16(d)—informal 2

Table 4 Numerical results of Succolarity of formal 1: Figs. 17 and 19

Dividing factor	Succolarity ( $\times 10$ )				Medium
	b2t	t2b	l2r	r2l	
270	3.489	3.023	3.33	3.415	3.314
135	3.489	3.023	3.33	3.415	3.314
90	3.489	3.023	3.33	3.415	3.314
54	3.489	3.023	3.33	3.415	3.314
45	3.489	3.023	3.33	3.415	3.314
30	3.489	3.024	3.33	3.415	3.315
27	3.488	3.023	3.33	3.415	3.314
18	3.489	3.026	3.33	3.413	3.314
15	3.487	3.024	3.33	3.413	3.314
10	3.486	3.028	3.331	3.407	3.313
9	3.489	3.033	3.339	3.414	3.319
6	3.482	3.035	3.339	3.412	3.317
5	3.473	3.035	3.313	3.38	3.3
3	3.487	3.075	3.357	3.384	3.326
2	3.43	3.085	3.4	3.354	3.317

image named H53022B, Fig. 23, there is an internal carotid artery plaque, on the second H53031B, Fig. 24, there is an internal carotid artery occlusion. Parts of the original image that contains only textual information were removed from the two images. The result images are both  $480 \times 240$  pixels.

In Figs. 23(a) and 23(b) it is not easy to visualize the occlusion that occurs in Fig. 24(b) and does not occur in Fig. 24(a). These images were submitted to heuristic tests to determine good values of threshold. The results of the threshold of these images are shown in Figs. 24(a) and 24(b).

After the threshold, it is easier to note that Fig. 24(b) has a complete occlusion and Fig. 24(a) has a partial obstruction. The next two images, Figs. 25(a) and 25(b), show the intermediate images generated during the executing of the method proposed to calculate the Succolarity of the input image in Fig. 24(a).

**Table 5** Numerical results of Succolarity of formal 2: Figs. 17 and 20

Dividing factor	Succolarity ( $\times 10$ )				
	b2t	t2b	l2r	r2l	Medium
270	3.432	3.364	2.752	3.152	3.175
135	3.432	3.364	2.752	3.152	3.175
90	3.432	3.364	2.752	3.152	3.175
54	3.432	3.364	2.752	3.152	3.175
45	3.432	3.364	2.751	3.152	3.175
30	3.431	3.364	2.753	3.152	3.175
27	3.432	3.364	2.752	3.151	3.175
18	3.431	3.364	2.753	3.151	3.175
15	3.428	3.362	2.754	3.152	3.174
10	3.424	3.361	2.754	3.147	3.172
9	3.415	3.354	2.756	3.148	3.168
6	3.41	3.355	2.758	3.145	3.167
5	3.408	3.358	2.755	3.139	3.165
3	3.326	3.294	2.783	3.121	3.131
2	3.295	3.286	2.847	3.113	3.135

**Table 6** Numerical results of Succolarity of informal 1: Figs. 17, 18 and 21

Dividing factor	Succolarity ( $\times 10$ )				
	b2t	t2b	l2r	r2l	Medium
270	2.87	0.543	0.317	3.113	1.711
135	2.87	0.543	0.317	3.113	1.711
90	2.87	0.543	0.317	3.113	1.711
54	2.87	0.543	0.318	3.113	1.711
45	2.87	0.543	0.317	3.113	1.711
30	2.869	0.543	0.318	3.113	1.711
27	2.869	0.544	0.319	3.112	1.711
18	2.868	0.546	0.321	3.111	1.711
15	2.866	0.547	0.322	3.112	1.712
10	2.861	0.553	0.327	3.113	1.711
9	2.862	0.556	0.333	3.104	1.714
6	2.845	0.568	0.35	3.086	1.712
5	2.828	0.574	0.358	3.107	1.717
3	2.765	0.645	0.424	3.03	1.716
2	2.595	0.823	0.637	2.867	1.73

The two following images, Figs. 26(a) and 26(b), show the intermediate images generated during the executing of the method proposed to calculate the Succolarity for the input image in Fig. 24(b).

The  $\ln \times \ln$  plots of the Succolarity are shown in Figs. 27 and 28.

Table 8 shows the Succolarity numerical values for the image H53022B, Fig. 23(a). Table 9 shows the Succolarity numerical values for the image H53031B, Fig. 23(b).

**Table 7** Numerical results of Succolarity of informal 2: Figs. 18 and 22

Dividing factor	Succolarity ( $\times 10$ )				
	b2t	t2b	l2r	r2l	Medium
270	1.768	0.189	0.332	0.469	0.69
135	1.768	0.189	0.332	0.469	0.69
90	1.768	0.189	0.332	0.469	0.69
54	1.768	0.19	0.332	0.469	0.69
45	1.768	0.19	0.333	0.468	0.69
30	1.767	0.19	0.333	0.468	0.69
27	1.767	0.191	0.333	0.468	0.69
18	1.765	0.19	0.334	0.467	0.689
15	1.764	0.193	0.336	0.466	0.69
10	1.757	0.195	0.336	0.463	0.688
9	1.757	0.199	0.334	0.461	0.688
6	1.742	0.207	0.349	0.453	0.688
5	1.723	0.217	0.358	0.448	0.686
3	1.6	0.234	0.373	0.414	0.655
2	1.44	0.287	0.47	0.373	0.642

**Table 8** Numerical values of Succolarity of the threshold H53022B, Fig. 23(a).  $d$  is the factor of division,  $BS$ , the box size (width  $\times$  height)

$d$	$\ln(d)$	$BS$	Succolarity ( $\sigma$ )		$\ln(100 \times \sigma)$	
			l2r	r2l	l2r	r2l
8	2.0794	(30 $\times$ 17)	0.4014	0.4169	3.6924	3.7303
4	1.3863	(60 $\times$ 34)	0.3993	0.4138	3.6871	3.7228
2	0.6931	(120 $\times$ 68)	0.3913	0.4036	3.6669	3.6978

**Table 9** Numerical values of Succolarity of the threshold H53031B, Fig. 23(b).  $d$  is the factor of division,  $BS$ , the box size (width  $\times$  height)

$d$	$\ln(d)$	$BS$	Succolarity ( $\sigma$ )		$\ln(100 \times \sigma)$	
			l2r	r2l	l2r	r2l
4	1.3863	(61 $\times$ 34)	0.1631	0.4306	2.7918	3.7626
2	0.6931	(122 $\times$ 68)	0.188	0.4181	2.9339	3.7331

The direction considered on the results was only horizontal because the vessels on the images are on this direction. In the non occluded image the results on the curve to l2r and r2l almost match as we can see by Fig. 27. However, when an obstacle is present on the analyzed image, the l2r and r2l curves differs significantly as could be seen in Fig. 28.

### 5 Conclusion

In this work, an approach to evaluate the fractal measure of Succolarity was presented. An equation to evaluate this measure was proposed based on the notions of directional

**Fig. 23** Carotid images from the vascular-web database [14]: (a) H53022B—Internal carotid artery plaque; and (b) H53031B—Internal carotid artery occlusion

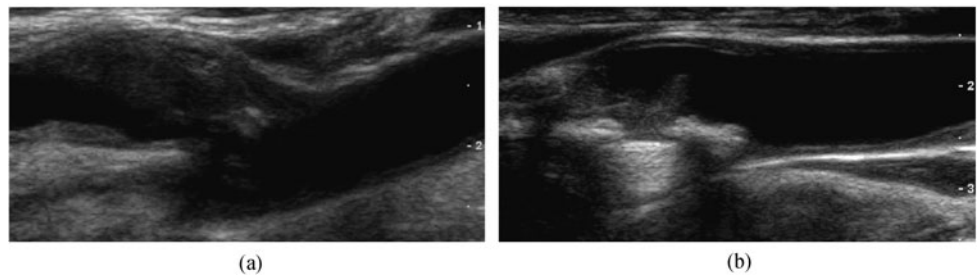


**Fig. 24** Thresholded images of images in Fig. 23: (a) Value of threshold heuristically chosen was 18; and (b) Value of threshold heuristically chosen was 15

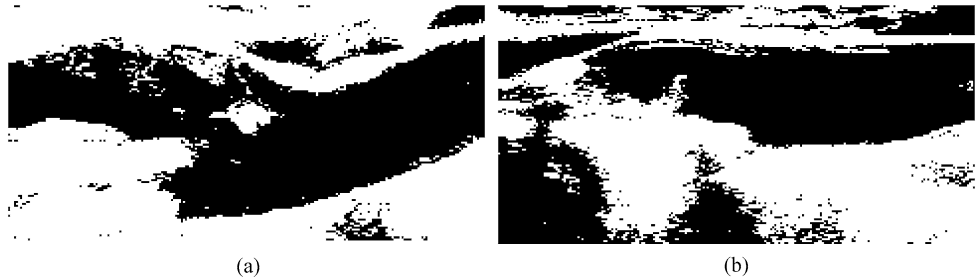


**Fig. 25** Intermediate images from the processing of image in Fig. 24(a): (a) for the direction *left to right* (l2r); and (b) for the direction *right to left* (r2l)

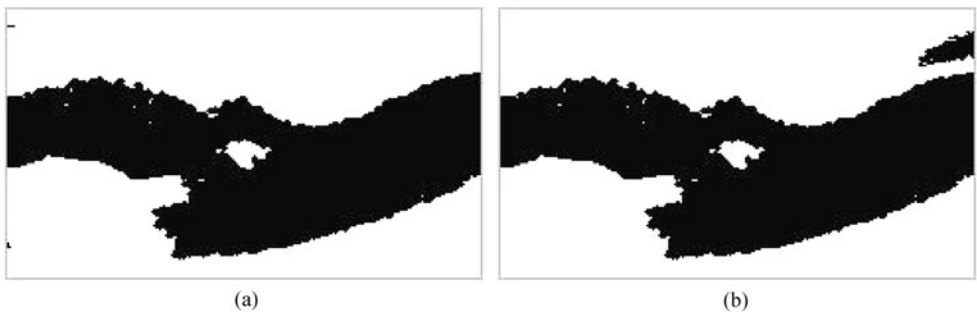
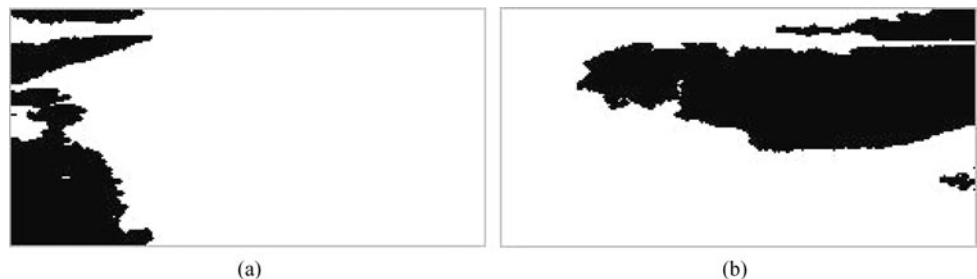


**Fig. 26** Intermediate images from the processing of image in Fig. 24(b) (a) for the direction *left to right* (l2r); and (b) for the direction *right to left* (r2l)



pressure due to percolation of a fluid in a partially penetrable environment.

How to compute the Succolarity from binary 2D and 3D digital images were discussed through examples.

Like the Lacunarity, our proposal to Succolarity computation considers the use of bi logarithm ( $\ln \times \ln$ ) or linear  $\times \log$  plots instead of a single value. The Succolarity values over different box sizes could give essential information useful to the pattern recognition process.

The results of the experiments on real images show that the method is very useful as a new feature to integrate other characteristics on pattern recognition processes. The notions of Succolarity [1] were respected and the measure could be

seen as a natural evolution of the FD and Lacunarity. The other advantage of the method is to be simple, easy and fast to be calculated.

The analysis of satellite images of cities over its social aspects using the Lacunarity is better than using FD [11, 12]. The method proposed here describes another approach that could differentiate not only between formal and informal areas like does the Lacunarity in [11, 12], but between different kinds of informal areas too.

The analysis of the vascular medical images indicates that the Succolarity is useful on determining vascular obstructions in ultrasound exams and strength the argument

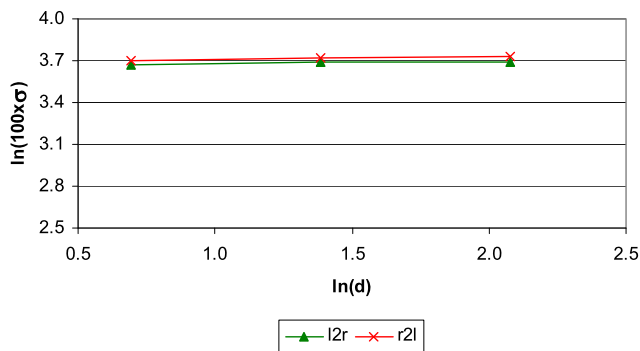


**Fig. 27**  $\ln \times \ln$  plot of the Succolarity for Fig. 24(a)

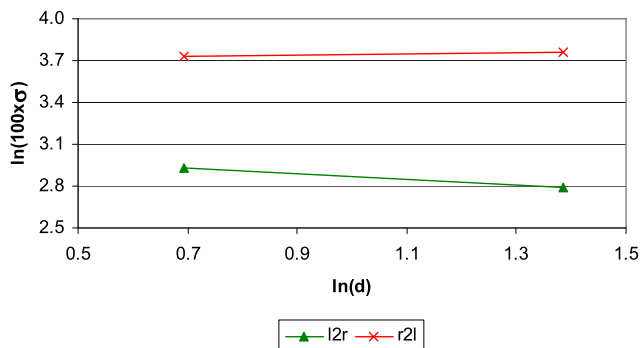


**Fig. 28**  $\ln \times \ln$  plot of the Succolarity for Fig. 24(b)

that directional information on images could be very well extracted by this method.

The main gain of using the Succolarity is that the method enables not one, but lots of ways to analyze the results, as could be seen by the two kinds of applications in this work, once the user knows something about what kind of information he wants to extract from the image, more he can take advantage of the representation of the result. The user could use different directions, combining it or not, depending on the problem in question. These were illustrated by the cities results of Succolarity, which uses four directions, and the vascular medical images results, that use only two directions. Succolarity is a great measure, which is very useful, not only for the type of images used here, but to generic images, that present some information associated with direction or flow. Among the applications are the study of percolation of petroleum and natural gas through semi-porous rock; where the theory can help to predict and improve the productivity of natural gas and oil.

**Acknowledgements** This work has been supported by CAPES, the Brazilian government agency.

## References

- Mandelbrot, B. B. (1977). *Fractal geometry of nature*. New York: Freeman.
- Melo, R. H. C. (2007). *Using fractal characteristics such as fractal dimension, Lacunarity and Succolarity to characterize texture patterns on images*. Master's thesis, Federal Fluminense University. Link: [http://www.ic.uff.br/~rmelo/msc\\_thesis.htm](http://www.ic.uff.br/~rmelo/msc_thesis.htm).
- Melo, R. H. C., Vieira, E. A., & Conci, A. (2006). Comparing two approaches to compute Lacunarity of mammograms. In *Proceedings of the IEEE signal processing society 13th international conference on systems, signal and image processing and semantic multimodal analysis of digital media (IWSSIP 2006)*, Budapest, Hungary (pp. 299–302).
- Melo, R. H. C., Vieira, E. A., & Conci, A. (2006). Characterizing the Lacunarity of objects and image sets and its use as a technique for the analysis of textural patterns. In J. Blanc-Talon, et al. (Eds.), *LNCIS: Vol. 4179. Advanced concepts for intelligent vision systems* (pp. 208–219). Berlin: Springer.
- Sarkar, N., & Chaudhuri, B. B. (1992). An efficient approach to estimate Fractal Dimension of textural images. *Pattern Recognition*, 25, 1035–1041.
- Block, A., von Bloh, W., & Schellnhuber, H. J. (1990). Efficient box-counting determination of generalized Fractal Dimensions. *Physical Review A*, 42, 1869–1874.
- Barabási, A. L., & Stanley, H. E. (1995). *Fractal concepts in surface growth*. New York: Cambridge University Press.
- Conci, A., & Monteiro, L. H. (2000). Multifractal characterization of texture-based segmentation. In *ICIP 2000*, Vancouver, Canada (pp. 792–795).
- Conci, A., & Proença, C. B. (1998). In *Computer networks and ISDN Systems, pages: Vol. 30. A fractal image analysis system for fabric inspection based on a box-counting method* (pp. 1887–1895). Amsterdam: Elsevier.
- Mandelbrot, B. B., & Van Ness, J. (1968). Fractional Brownian motion, fractional noise and applications. *SIAM Review*, 10, 422–437.
- Barros Filho, M. N. M., & Sobreira, F. A. (2005). *Assessing texture pattern in slums across scales: an unsupervised approach*. CASA working paper, Centre for Advanced Spatial Analysis, CASA Seminar, University College London, London, 87. Link: [http://www.casa.ucl.ac.uk/working\\_papers/paper87.pdf](http://www.casa.ucl.ac.uk/working_papers/paper87.pdf).
- Barros Filho, M. N. M., & Sobreira, F. A. (2005). *Analysing spatial patterns in slums: a multiscale approach*. Congresso Internacional de Planejamento Urbano Regional Integrado e Sustentável, São Carlos (SP). São Carlos: PLURIS.
- Melo, R. H. C., & Conci, A. (2008). Succolarity: defining a method to calculate this fractal measure. In *15th international conference systems, signals and image processing, 2008. IWSSIP 2008*, Bratislava, Slovak Republic (pp. 291–294).
- Size, G. P., & Duncan, R. K. (2006). Vascular-web. Link: <http://www.vascular-web.com>, 2006.
- Batty, M., & Longley, P. (1994). *Fractal cities: geometry of form and function* (1st ed.). London: Academic Press.
- Frankhauser, P. (1997). Fractal analysis of urban structures. In E. Holm (Ed.), *Modelling space and networks: progress in theoretical and quantitative geography* (pp. 145–181). Umea: Gerum Kulturgeografi.
- Sobreira, F., & Gomes, M. (2001). *The geometry of slums: boundaries, packing and diversity*. Working paper series, CASA—Centre for Advanced Spatial Analysis—University College London, London, 30. Link: [http://www.casa.ucl.ac.uk/working\\_papers/paper30.pdf](http://www.casa.ucl.ac.uk/working_papers/paper30.pdf).
- Space Imaging Brazil (2004). Link: <http://www.spaceimaging.com.br/>.
- Barros Filho, M. N. M., & Sobreira, F. J. A. (2008). Accuracy of Lacunarity algorithms in texture classification of high spatial resolution images from urban areas. In *XXI congress of international society of photogrammetry and remote sensing, 2008, Beijing, China. XXI congress of international society of photogrammetry and remote sensing*, Beijing, China.

20. Valous, N. A., Mendoza, F., Sun, D.-W., & Allen, P. (2009). Texture appearance characterization of pre-sliced pork ham images using fractal metrics: Fourier analysis dimension and Lacunarity. *Food Research International*, 42(3), 353–362.
21. Frankhauser, P. (2008). Fractal geometry for measuring and modelling urban patterns. In S. Albeverio, D. Andrey, P. Giordano, & A. Vancheri (Eds.), *The dynamics of complex urban systems—an interdisciplinary approach* (pp. 241–243). Berlin: Springer.
22. Tannier, C., & Pumain, D. (2005). Fractals in urban geography: a theoretical outline and an empirical example, Cybergeog. *European Journal of Geography*, 307, 20 <http://www.cybergeog.eu/index3275.html>, 22 pp.



**R.H.C. de Melo** received his M.Sc. in Computer Science from Federal Fluminense University (UFF) at Niterói (Brazil) in 2007. He is currently a project manager and researcher at ADDLabs (The Artificial Intelligent laboratory of UFF). His major research interest includes image processing, image analysis, pattern recognition and computer vision (<https://sites.google.com/site/rhcmelo/>).



**A. Conci** received M.Sc. and D.Sc. degrees in civil engineering from PUC-Rio, Brazil, in 1983 and 1988, respectively. Since 1994 she has been a titular professor at the Federal Fluminense University, first in Mechanical Engineer Department and now in Computer Science Department. Her major research interests are in Computer Graphics, Image Processing and Biomechanics (<http://www.ic.uff.br/~aconci>).